Quaternary Science Reviews 71 (2013) 191–204

Contents lists available at SciVerse ScienceDirect

Quaternary Science Reviews

journal homepage: www.elsevier.com/locate/quascirev

# Microsedimentological characterization using image analysis and μ-XRF as indicators of sedimentary processes and climate changes during Lateglacial at Laguna Potrok Aike, Santa Cruz, Argentina

Guillaume Jouve [a,b,*], Pierre Francus [a,b], Scott Lamoureux [c], Laurence Provencher-Nolet [a], Annette Hahn [d], Torsten Haberzettl [e], David Fortin [a,b], Laurence Nuttin [a,b], The PASADO Science Team [1]

[a] Centre Eau, Terre et Environnement, Institut National de la Recherche Scientifique, Québec, Québec G1K 9A9, Canada
[b] GEOTOP Research Center, Montréal, Québec H3C 3P8, Canada
[c] Department of Geography, Queen's University, Kingston, Ontario K7L 3N6, Canada
[d] Geomorphology and Polar Research (GEOPOLAR), Institute of Geography, University of Bremen, Celsiusstr. FVG-M, D-28359 Bremen, Germany
[e] Physical Geography, Institute of Geography, Friedrich-Schiller University Jena, Löbdergraben 32, D-07743 Jena, Germany

ARTICLE INFO

*Article history:*
Received 9 November 2011
Received in revised form
23 May 2012
Accepted 4 June 2012
Available online 17 July 2012

*Keywords:*
Sedimentary processes
XRF
Image analysis
Granulometry
Micropumices
Paleoclimate

ABSTRACT

Palaeoclimatic and paleoenvironmental high latitude records in the Southern Hemisphere are scarce compared to the northern counterpart. However, understanding global evolution of environmental systems during sudden climate changes is inseparable from an equivalent knowledge of both Hemispheres. In this context, a high-resolution study of lacustrine sediments from Laguna Potrok Aike, Santa Cruz province, Patagonia, Argentina, was conducted for the Lateglacial period using concurrent X-Ray Fluorescence (XRF) and Scanning electron microscope analyses. Peaks of Ca/Si and Mn, and occurrences of the green alga *Phacotus lenticularis* have been interpreted as variations in ventilation of the water column from 13.6 to 11.1 ka cal. BP. During this interval, mild climate conditions during the Younger Dryas are characterized by relatively weak westerlies favouring the formation of a stratified water body as indicated by preserved manganese and Ca/Si peaks and high Total Organic Carbon (TOC) values. In this environment, water in the epilimnion can reach sufficiently high temperature to allow *P. lenticularis* to grow. Colder conditions are marked by peaks in Ca without *P. lenticularis* and occur during the Antarctic Cold Reversal (ACR). In this Lateglacial interval, micropumices were also detected in large amount. Image analysis of thin sections allowed the counting and size measurement of detrital particles and micropumices separately. Micropumices significantly influence the iron and titanium content, hence preventing to use them as proxies of detrital input in this interval.



## 1. Introduction and scientific context

Since the SALSA project (South Argentinean Lake Sediment Archives and modelling) initiated within the framework of the German Climate Research Program (DEKLIM), Laguna Potrok Aike (51°58′S, 78°23′W) has revealed a unique opportunity to reconstruct paleohydrological and paleoenvironmental conditions for the mid to high latitude of the southern part of South America, and resulted in the completion of a deep drilling in the context of ICDP (introduction paper of this issue). This paper aims at providing a high-resolution sedimentological and hydrological reconstruction of Laguna Potrok Aike during the Lateglacial period between 15.59 and 10.46 ka cal. BP. This interval is of particular interest because relatively few high-resolution and well-dated Lateglacial records exist in the Southern hemisphere in comparison with the Northern Hemisphere. However, several recent contributions (Gilli et al., 2001, 2005a, 2005b; Markgraf et al., 2003; Glasser et al., 2004; Haberzettl et al., 2005, 2007, 2009; Mayr et al., 2005; Villa-Martínez and Moreno, 2007; Whitlock et al., 2007; Unkel et al., 2008; McGlone et al., 2010; Siani et al., 2010) contributed to the understanding of the potential leads and lags of global climate variations (Labeyrie et al., 2004; Pedro et al., 2011), especially

* Corresponding author. Tel.: +1 418-654-4480x4480; fax: +1 418 654 2600.
*E-mail addresses:* guillaume.jouve@ete.inrs.ca (G. Jouve), pfrancus@ete.inrs.ca (P. Francus), Scott.Lamoureux@queensu.ca (S. Lamoureux), alphie_007@hotmail.com (L. Provencher-Nolet), anhahn@uni-bremen.de (A. Hahn), Torsten.Haberzettl@uni-jena.de (T. Haberzettl), david.fortin@ete.inrs.ca (D. Fortin), lanuttin@gmail.com (L. Nuttin).
[1] PASADO Science Team as listed at http://www.icdp-online.org/front_content.php?idcat=1494.

0277-3791/$ – see front matter © 2012 Elsevier Ltd. All rights reserved.
http://dx.doi.org/10.1016/j.quascirev.2012.06.003

during rapid cold or warm events such as the Antarctic Cold Reversal (ACR) and Younger Dryas (YD) chronozones.

Ice cores from Vostok and EPICA Dome C in Antarctica provided several palaeoclimatic proxies such as the hydrogen ($\delta D$) and oxygen ($\delta^{18}O$) isotopes as indicators of changes in temperature and ice volume (Jouzel et al., 1987) for multiple interglacial–glacial cycles. Moreover, these records also contain a proxy for the amount of atmospheric dust, the nss-$Ca^{2+}$ (Röthlisberger et al., 2002) that has been demonstrated to come mainly from Patagonia (Basile et al., 1997). Sugden et al. (2009) showed that dust levels measured in the EPICA Dome C ice cores in Antarctica (Röthlisberger et al., 2002) originated from the glacial outwash in Patagonia and more specifically between 52°48′S and 53°36′S, a region near Laguna Potrok Aike located at 51°59′S. Their work suggested that peaks observed in the Antarctic cores coincide with periods when glaciers were advancing in Patagonia, and rivers were depositing sediments in outwash plains. After dewatering, they were deflated by the intense westerly winds and transported to Antarctica. Also during glacial periods, the continental shelf was larger because low sea level exposed more surface area for deflation. Conversely, when glaciers melted, sediments were trapped at the bottom of large lakes, hence were protected from wind erosion. Basile et al. (1997) showed that the period of fastest sea level rise, approximately 14 ka cal. BP (Guilderson et al., 2000) coincides with a period without changes in dust input at Dome C. It either means that shelf was not an important source of dust for Antarctica or that the main vector of dust transport towards Antarctica, i.e. westerlies at high latitude in southern part of South America (Basile et al., 1997), were substantially reduced during Lateglacial. Nevertheless, it had been proved that Australian aeolian dust was also an important source of dust for the Eastern part of the Antarctic continent during interglacial periods (Revel-Rolland et al., 2006). During glacial periods, South America would remain the dominant source for dust input in East Antarctica.

Climate reconstructions of the southern hemisphere remain scarce. McGlone et al. (2010) presented a reconstruction of summer temperature for Campbell Island, in the Southern Ocean, over the past 16.5 ka cal. BP based on fossil pollen, and proposed a general pattern of climate evolution for the entire southern South Hemisphere since the deglaciation. They concluded that although mean annual temperatures may have been close to or even warmer than today in the latter part of the Lateglacial and the early Holocene, summer temperatures certainly were cooler (McGlone et al., 2010). However, they also suggested that terrestrial proxies beyond 50°S during the Lateglacial to the early Holocene should not be interpreted in terms of temperature and humidity. Instead, these studies more reflect the position of the westerly wind belt and the associated general pattern of precipitation (Schneider et al., 2003; Mayr et al., 2007) during Lateglacial in the southern South America. Hence, in Eastern Patagonia, the more westerlies are weak the more precipitations coming from Atlantic are important (Schneider et al., 2003; Mayr et al., 2007). Given that the sediments of Laguna Potrok Aike recorded environmental and climatic variations (Haberzettl et al., 2005, 2007; Mayr et al., 2007; Wille et al., 2007), they offer the opportunity to verify and refine our understanding of hydroclimatic conditions during two key periods, i.e. the ACR, from 14.8 to 13 ka cal. BP as defined by Pedro et al. (2011), and the YD, from 12.7 to 11.6 ka cal. BP as defined by Lowe et al. (2008).

Here, we report high-resolution μ-XRF core scanner geochemical measurements along with observations and analyses of Scanning Electron Microscope (SEM) images of sediment thin-sections and compare them with new other data from the PASADO project (this issue) to revisit paleoclimate interpretations during Lateglacial. The interpretation of elements widely used as indicators of past hydrological and paleoredox conditions in sediments (Haug et al., 2003; Demory et al., 2005; Eusterhues et al., 2005), including at Laguna Potrok Aike (Haberzettl et al., 2007), are refined in the light of microscopic investigation of sedimentary fabric (Francus and Karabanov, 2000). The latter are supported by SEM–EDS (Scanning Electron Microscope–Energy Dispersive X-ray Spectroscopy) analyses allowing the identification of the mineral phases containing the elements detected by μ-XRF.

## 2. Regional setting

Laguna Potrok Aike is located in Argentina, southeast Patagonia near the border with Chile (Fig. 1). The lake was created several hundred thousand years ago after a phreatomagmatic eruption, i.e. an explosive volcanic eruption caused by the contact between a rising magma and groundwater (Skewes, 1978). The crater resulting from this eruption is currently filled by a lake that acted as a sediment trap. The climate of this region is dominated by strong westerly winds that can reach monthly average speeds of 9 m $s^{-1}$ at the beginning of summer (Endlicher, 1993). The wind action mixes the water throughout the year, preventing stratification during summer and the formation of ice cover in winter (Endlicher, 1993; Zolitschka et al., 2006). The lake is almost circular and has a maximum diameter of 3470 m. The watershed is approximately 200 $km^2$, but is mostly limited to episodic surface water flows that only occur through the ravines and canyons. Currently, the lake has no outlet, which makes it very sensitive to changes in water balance (evaporation/precipitation): high lake level correspond to wetter climate conditions and low lake levels occur during dry periods (Haberzettl et al., 2005). In summer 2002, lake level was at 113 m above sea level and maximum water depth was 100 m. The lake is

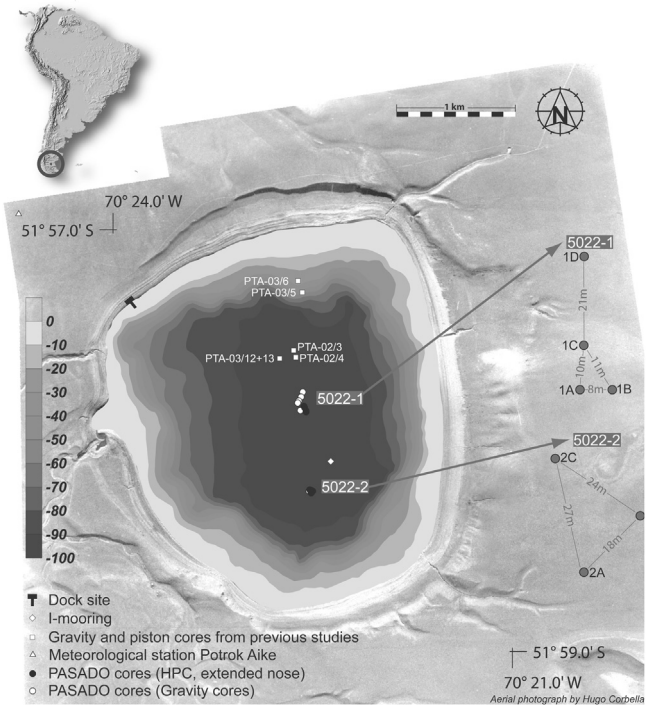


**Fig. 1.** Location of Laguna Potrok Aike in southern Patagonia (circle on inset map of South America). Aerial photograph of the immediate catchment area of Laguna Potrok Aike (kindly provided by Hugo Corbella, Buenos Aires) and bathymetric map of the lake with indicated coring sites. Black dots indicate the positions of piston cores; white dots mark the position of gravity cores. Lateral distance between coring positions of one site is between 8 and 24 m (modified from Ohlendorf et al., 2011).

bordered by several paleo-terraces (Haberzettl et al., 2005) that indicate past water level variations over time.

## 3. Materials and methods

### 3.1. Field studies and composite sedimentary sequence

Lake drilling at Laguna Potrok Aike was conducted from August to November 2008 using the GLAD800 drilling system. Cores were mainly recovered using a hydraulic piston core system at two primary sites: 5022-1 (PTA 1) and 5022-2 (PTA 2) (Fig. 1) (Ohlendorf et al., 2011). Average core recovery was around 92.1% in the hole site 5022-1 and 98.8% in the hole site 5022-2. A total of 533 m of cores were obtained reaching a maximum depth of 101.5 m blf (below lake floor) at the deepest location (Zolitschka et al., 2009a; Ohlendorf et al., 2011). A 106.9 m-long composite profile, later explained in meter composite depth (m cd), from site 5022-2 was constructed using the best sections of the tree holes (A, B and C) (Fig. 1) by correlating stratigraphic markers and facies and magnetic susceptibility of each hole (Kliem et al., 2013). This profile is considered as the reference sedimentary sequence by scientists involved in the Potrok Aike Sediment Archive Drilling prOject (PASADO). Most of the sediments are made of silty clay/clayey silt or sand (Zolitschka et al., 2009a). About 50% of the entire composite sequence are redeposited (Zolitschka et al., 2009b) and were removed from the composite sequence.

Slightly more than 2 m were subsampled in high-resolution, thin-section and u-channels (see details below in part 3.2), from 16.303 to 14.058 m cd (from 15.59 to 10.48 ka cal. BP) and correspond to a partially laminated interval. These sediments are located 48 cm above a 1.5 m-thick interval consisting of alternations of (1) highly altered tephra of unknown origin, white layers of volcaniclastic laminations (cm-scale), and (2) brown laminations of fine sand with organic macroremains (cm-scale). These remains of aquatic macrophytes were already found and described in Haberzettl et al. (2007). The Reclus tephra (1 cm thick), deposited around 16 ka cal. BP ago (Kliem et al., 2013), is situated just at the top of this 1.5 m-thick interval, i.e. 20 cm below our sampled interval.

### 3.2. Methods

All subsampling operations were coordinated with the PASADO Science Team (Ohlendorf et al., 2011). Sediments were subsampled for thin-sections using aluminium slabs directly from the composite profile or from equivalent core sections (Francus and Asikainen, 2001). These slabs were freeze-dried and impregnated with Spurr's low velocity epoxy resin (Lamoureux, 1994), and thin-sections were prepared commercially. They were then scanned in natural and cross-polarized light using a flatbed transparency scanner (De Keyser, 1999; Lamoureux and Bollmann, 2004). Images retrieved in high-resolution (2400 dpi) were imported into image analysis software developed at INRS-ETE (Francus and Nobert, 2007) that allows the selection of regions of interest (ROI) from the flatbed scan images and the automated acquisition of SEM images of those ROIs. Image analysis of backscattered electron (BSE) images of thin-sections involves the transformation of the initial grey-scale image into a black and white image marking out the sedimentary particles in their matrix (Francus, 1998). Then, the following measurements were made on each particle: center of gravity, area, length of major axis, and minor axis of the best fitting ellipse and angle of major axis with the horizontal. These measurements were then recorded in a spreadsheet for further processing (Table 1) (Francus and Karabanov, 2000) and the calculation of grain-size parameters (Francus et al., 2002). Details of the algorithms used here are available in annex 1. Initially, the software weights each particle by considering them as spherical quartz grains (Francus et al., 2002). Weight is calculated using the formula: $((4/3)^*\pi^*((D_0/2)^3))^*2.65$, with $D_0$ representing the apparent disk diameter. Then, particles weight is summed for each particle size class (Table 1) so classes' percentages can be

**Table 1**
Grain size results, with or without micropumices, extract from the image analysis software. $n$ = number of particles, $P\%$ = total percentage of area of black pixels (representing all particles detected) per image. Particle size (μm): each particle size range and its weight (μg) associated per image. Micropumices (%): percentage of micropumices among all particles detected.

| | | IA1 (Fig. 3) | | IA2 (Fig. 3) | |
|---|---|---|---|---|---|
| | | With micropumices | Without micropumices | With micropumices | Without micropumices |
| | $n$ | 765 | 739 | 1661 | 940 |
| | $P\%$ | 9.446 | 8.47 | 32.761 | 17.206 |
| Particle size (μm) | 2.423–2.920 | 0 | 0 | 0 | 0 |
| | 2.920–3.519 | 0 | 0 | 0 | 0 |
| | 3.519–4.241 | 15,595.845 | 15,235.228 | 22,604.272 | 13,749.995 |
| | 4.241–5.111 | 18,442.661 | 18,065.163 | 27,573.769 | 16,805.741 |
| | 5.111–6.158 | 24,715.816 | 24,249.405 | 45,456.795 | 25,534.073 |
| | 6.158–7.421 | 42,634.015 | 42,481.375 | 74,166.548 | 43,436.702 |
| | 7.421–8.944 | 48,919.027 | 44,748.335 | 109,660.789 | 56,827.236 |
| | 8.944–10.780 | 84,744.175 | 82,499.008 | 212,826.22 | 111,644.902 |
| | 10.780–12.990 | 100,070.15 | 88,445.909 | 333,008.326 | 182,091.608 |
| | 12.990–15.650 | 94,682.106 | 97,396.872 | 542,091.705 | 282,375.983 |
| | 15.650–18.860 | 98,742.516 | 102,957.765 | 630,415.157 | 381,583.453 |
| | 18.860–22.730 | 134,712.246 | 140,966.221 | 543,035.155 | 312,355.25 |
| | 22.730–27.380 | 396,186.424 | 345,135.252 | 1,167,362.394 | 690,559.947 |
| | 27.380–33.000 | 384,242.334 | 184,280.941 | 1,313,125.718 | 642,931.37 |
| | 33.000–39.770 | 373,390.995 | 369,123.788 | 1,414,062.558 | 470,743.142 |
| | 39.770–47.930 | 393,557.113 | 388,270.455 | 1,563,340.26 | 838,658.877 |
| | 47.930–57.770 | 161,557.694 | 0 | 1415,943.477 | 1,220,551.665 |
| | 57.770–69.620 | 402,554.583 | 307,073.893 | 1,299,911.426 | 1,097,461.932 |
| | 69.620–83.900 | 1,315,369.583 | 1,360,918.122 | 3,478,764.48 | 1,022,495.704 |
| | 83.900–101.100 | 0 | 0 | 1,056,758.108 | 0 |
| | 101.100–121.800 | 0 | 0 | 0 | 0 |
| | Micropumices (%) | 3.4 | 0 | 43.4 | 0 |

calculated. Finally, the sediment is characterized according to the Krumbein and Sloss (1963) classification.

The examination of BSE images revealed the presence of numerous micropumices. We proceeded to two different counting, which are (1) manual detection of micropumices performed on BSE images and (2) measurement with image analysis (Francus, 2004). Because they sometimes represent a large proportion of the sediment, they were sorted into three size categories. The three size fractions were defined and chosen in order to take into account the difficulty to detect them in SEM cross-sections when they were smaller than 10 μm, and to be able to be subsequently compared them with grain size results: between 10 and 20 μm (fine silt), between 20 and 63 μm (medium silt to coarse silt), and between 63 and 200 μm (sand) (modified from Wentworth (1922) by Krumbein and Sloss (1963)).

The examination of BSE images also revealed the presence of *Phacotus lenticularis,* a green alga with a calcite lorica already described by Haberzettl et al. (2007). Only a qualitative estimation of its presence was performed: each BSE image was classified as *P. lenticularis* absent (0), scarce (1) or abundant (2).

Several ROIs were selected to cover facies including *P. lenticularis*, sedimentary fraction from clay to sand and micropumices and were analysed using an Energy Dispersive Spectroscopy (EDS) to qualitatively and semi-quantitatively characterize their chemical composition at the microscopic scale.

We used an ITRAX™ core scanner, with a molybdenum tube, that simultaneously acquires microdensity (radiography) and microgeochemical variations (XRF) of sediment cores using two separate X-ray detection systems (Croudace et al., 2006). The analysis is non-destructive. A resolution of 0.1 mm was conducted with an exposure time of 15 s. Voltage was 30 kV and current was 25 mA. Here, we analysed the u-channels sampled from the composite sections, which were taken for paleomagnetic analysis (Lisé-Pronovost et al., 2013). The numbers of counts for each element in each spectrum acquired for a specific depth interval was normalized by the total number of counts of that spectrum (expressed in kcps, i.e. 1000 counts per second). “inc” is the incoherent scattering or Compton scattering and “coh” is the coherent or Rayleigh scattering. Rayleigh scattering is more important for samples containing elements with high *Z* number, Compton scattering is more important for samples containing elements with low *Z* number. Therefore, Inc/coh ratio is inversely proportional to the average atomic weight, and thus can be an indicator of the organic matter content, as demonstrated by Guyard et al. (2007) in Lake Bramant (French Alps), porosity and water content (Jenkins, 1999).

We used version 3 of the age model established by Kliem et al. (2013) for the last 16 ka cal. BP (Fig. 2). Our sampling resolution and the accuracy of the model allows for a decadal resolution of our geochemical and microfacies analyses. Water Content (%) and the Total Organic Carbon (%) measurements were achieved by GEOPOLAR group and belong to the PASADO Science Team (Fortin et al., 2013). Total Organic Carbon (TOC) samples were freeze-dried and ground using a mortar and pestle prior to the measurements. Concentrations of total carbon (TC) were determined by a CNS elemental analyzer (EuroEA). Samples for the measurement of TOC were pre-treated with 3% and 20% HCl at a temperature of 80 °C to remove carbonates and afterwards analysed by the same device. Water content was measured using standard volumes; a known volume of sample material was weighed, dried and reweighed. More specifically, volumetric samples were freeze dried in open vials for 45 h under a vacuum of $1.1 \times 10\ (-1)$ mbar using a Lyovac GT2 freeze-dryer (Steris GmbH, Huerth, Germany) (Fortin et al., 2013). The water content (WC) was ascertained by subtracting the net from the gross weight. This was converted into percentages.

## 4. Results

### 4.1. General stratigraphy

The study interval is divided in three units (I, II, III), and four subunits (IP, IIa, IIb and IIc). These were arbitrarily established based on their geochemistry (significant variations in μ-XRF, TOC and WC), and their content in micropumices and *P. lenticularis* occurrences (Fig. 3):

- Unit I from 16.303 to 15.580 m cd (15.59–13.64 ka cal. BP)
  - Subunit IP from 15.91 to 15.8 m cd (11 cm thick)
- Unit II from 15.580 to 14.740 m cd (13.64–11.64 ka cal. BP)
  - Subunit IIa from 15.52 to 15.38 m cd (14 cm thick)
  - Subunit IIb from 15.22 to 15.10 m cd (12 cm thick)
  - Subunit IIc from 14.97 to 14.80 m cd (17 cm thick)
- Unit III from 14.74 to 14.058 m cd (11.64–10.48 ka cal. BP).

Along this entire interval, sediment consists in very thin bedded to medium bedded, grain-supported, and angular to sub-rounded medium silt to fine sand. It is interrupted by a 6 cm thick bed of reworked sediments (4 cm reworked − 2 cm laminated − 2 cm reworked) in the middle of unit III (light grey lines R1 and R2 in Fig. 3) that were omitted from analyses.

### 4.2. Sedimentary facies

#### 4.2.1. Micropumices

Micropumices such as the ones described in Evans and Bradbury (2004) (Fig. 4A and B) appear all along the core sections studied. Micropumices are abundant in Unit I: ten to 150 particles of these micropumices from 10 μm to 150 μm are present in each image (Fig. 3D1). A peak is observed in subunit IP. In unit II, the amount of micropumices decreases but three peaks occur during subunit IIa, IIb and IIc in one or the other size fraction (Fig. 3D1). In unit III, the number of micropumices continues to decrease steadily.

Percentage of black pixels corresponding to micropumices in all particles detected with the image analysis software varies from: 0.7–43.4 % of particles for unit I (average = 11.8%), with one peak during subunit IP; 0.3–15.2% of particles for unit II (average = 3.1%), with three peaks during subunit IIa, IIb, and IIc; 0–4.5% of the particles for unit III (average = 0.6%) (Fig. 3D2).

#### 4.2.2. SEM and EDS

Fig. 5A shows SEM–EDS maps for sediments in unit II. Silicon is found in micropumices and detrital particles between 10 μm and 150 μm. Silicon is not present in *P. lenticularis,* which is found from 15.35 to 14.34 m cd, i.e. between 13 and 11 ka cal. BP. Titanium and Mn content is weak, while Fe content is more present in detrital particles but low in micropumices. In view 2 (unit I) micropumices are coloured in red to show an example of their high potential of concentration in sediments.

#### 4.2.3. Image analysis

Image analysis of a SEM image of a facies poor in micropumices, 3.4% only (Table 1), reveals that micropumices are mainly present in the medium to coarse silts fraction (Fig. 6D). Fig. 7A shows a similar view of a micropumices-rich facies from unit I (view 2 Fig. 3). The SEM image (Fig. 7A) reveals a matrix mainly composed of volcanic debris and glass splinters mostly represented by fragments of micropumices. Processed images B and C and corresponding particle-size plot better reveals the relative importance of micropumices: sample with all particles has a mode in the sand fraction, while the one without micropumice is centred on coarse silts (Fig. 7D).

### 4.3. Grain size

All three counted size fractions with micropumices (Fig. 8A) display similar variations along the three units compared to counts excluding micropumices (Fig. 8B). Correlations between each size fractions with and without micropumices are: $R^2 = 0.94$ for fine silts, $R^2 = 0.87$ for coarse silts and $R^2 = 0.88$ for fine sands. More specifically, the three fractions remain generally stable in unit I. In unit II, fine and coarse silts slightly decrease whereas fine sands slightly increase. In unit III, fine silts remain mostly stable, coarse silts generally increase while fine sands decrease.

### 4.4. Geochemistry

Calcium, Ti, Mn, Fe, and Si are the main elements detected here and that are further discussed in the frame of this study along with the inc/coh ratio (Fig. 3B).

Along our 2.26 m cd-long section (Fig. 3A), five discrete intervals have high Ca values, characterized by relative intensity three times more important than the average Ca intensity of the remaining interval (Fig. 3B). They are located between: 15.80 and 15.73 m cd (7 cm thick) in unit I, 15.52 and 15.38 m cd (14 cm thick) in subunit IIa, 15.22 and 15.10 m cd (12 cm thick) in subunit IIb, 14.97 and 14.80 m cd (17 cm thick) in subunit IIc and between 14.44 and 14.40 m cd (4 cm thick) in unit III.

Ca/Si show similar variability to that of Ca/kcps, except for unit I and III where it does not reveal any significant peak (Fig. 3B).

Three peaks of Mn occur within unit II (Fig. 3B). These are between: 15.52 and 15.38 m cd (14 cm thick) (subunit IIa), 15.18 and 15.10 m cd (8 cm thick) (subunit IIb), 14.90 and 14.80 m cd (10 cm thick) (subunit IIc). Variations in Fe content reveal different trends (Fig. 3B): in unit I, it is relatively low and stable, and shows a general rise from the base of unit II to the end of unit III. However, in unit II,

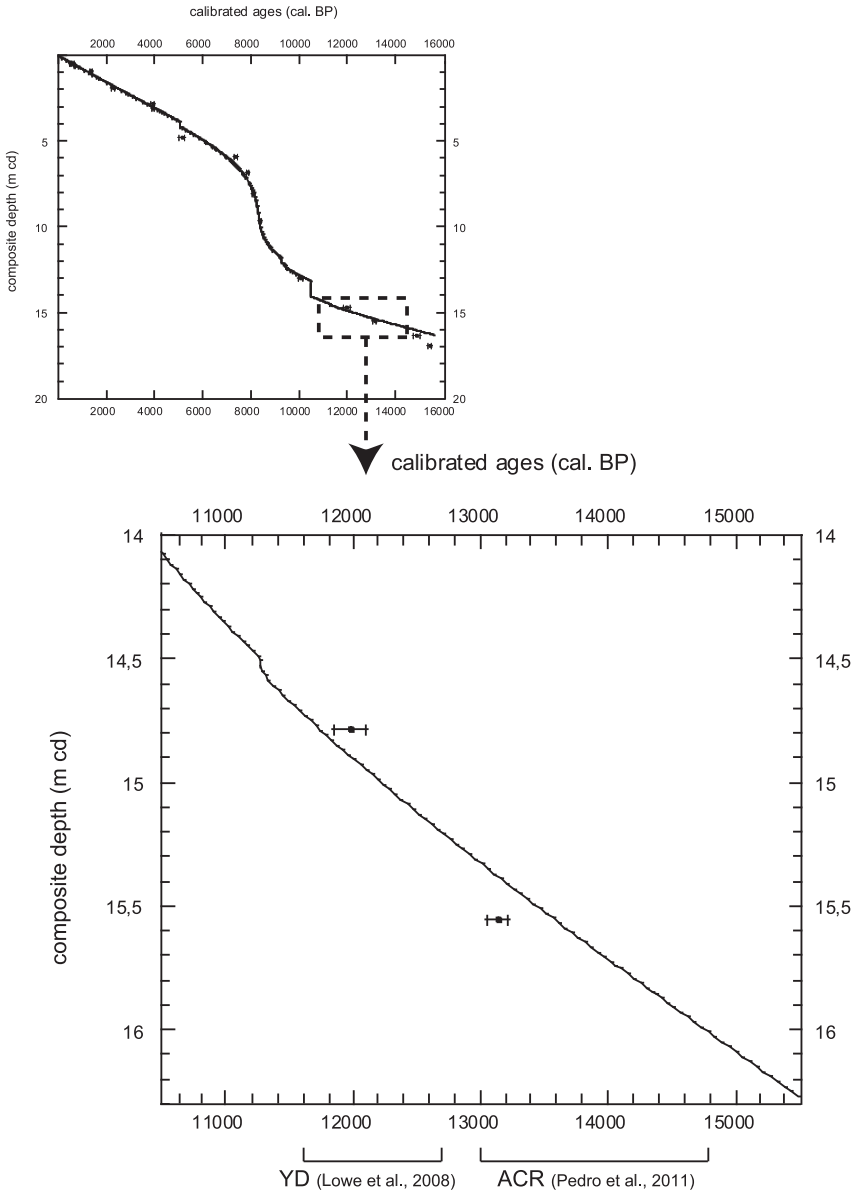


**Fig. 2.** Age model plotted with AMS radiocarbon ages (1σ error) from 5022-2CP of Laguna Potrok Aike calibrated (Kliem et al., 2013).

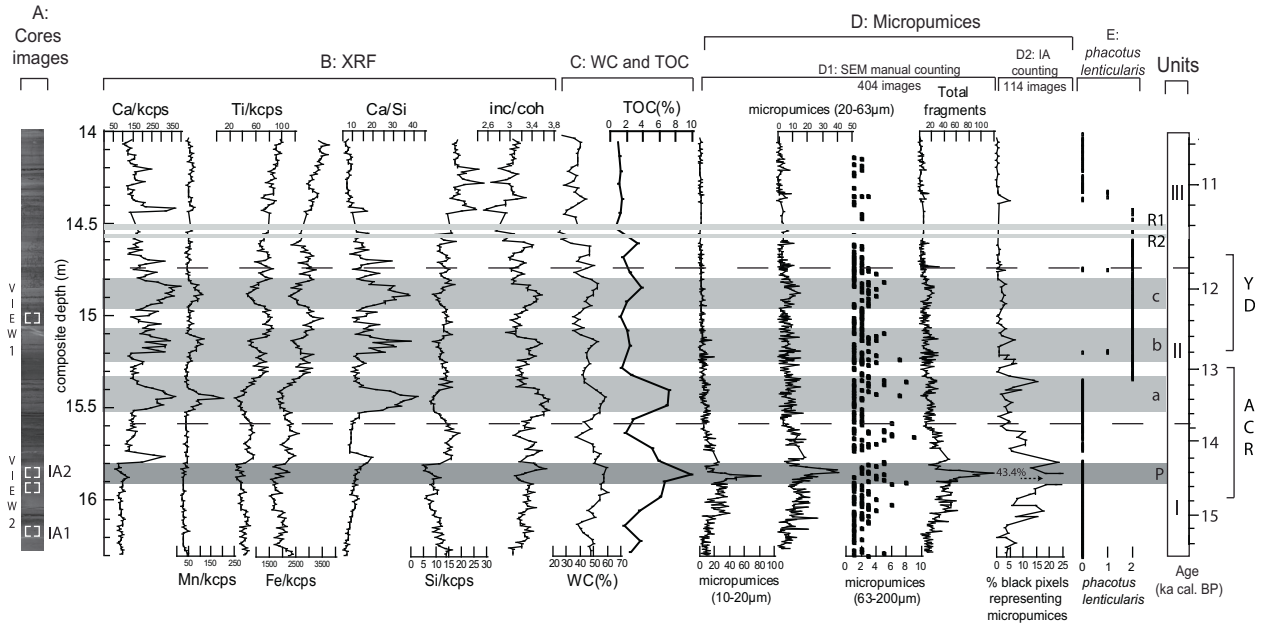


**Fig. 3.** A: sediment core photographs (source ICDP's Internal Data base), with the position of view 1 and 2 (SEM–EDS mapping image from Fig. 5A and B respectively), and the position of IA1 and IA2 (SEM–BSE-images from Figs. 6A and 7A). B: µ-XRF results. Inc/coh ratio is related to TOC and WC. C: WC (%) and TOC (%). D: occurrence of micropumices using (D1) SEM manual counting of micropumices performed on 404 BSE images; and (D2) image analysis (IA) grain-size measurements realized on 104 BSE images. E: occurrence of *Phacotus lenticularis* according to 3 classes: absence (0), the scarcity (1) and the abundance (2). Units are arbitrary and are based on geochemistry and microfacies data. Age scale on the right was constructed from the age model (version 3) established by Kliem et al. (2013) (Fig. 2). Light grey lines R1 and R2 represent the 4 and 2 cm thick beds of reworked sediments. Medium grey lines a, b and c: subunits in unit II. Dark grey line P: subunit in unit I representing the micropumices-rich interval. ACR and YD represent the Antarctic Cold Reversal and the Younger Dryas chronozones respectively.

three drops appear between: 15.60 and 15.30 m cd (30 cm thick) (subunit IIa), 15.20 and 15.12 m cd (8 cm thick) (subunit IIb), 14.95 and 14.80 m cd (15 cm thick) (subunit IIc). During unit III, Fe content shows a steady increase.

Titanium values show similar variability to that of Fe, although the steady rise in unit III is gentler (Fig. 3B).

In unit I (Fig. 3B), the inc/coh ratio profile shows an increase until subunit IP, where it reaches its highest values. Thereafter, it decreases slightly until the onset of unit II. In that unit, signal generally drops but three peaks occur in subunits IIa, IIb and IIc. In unit III, signal continues to decrease with a slight ascent at the end (Fig. 3B).

Total Organic Carbon values vary within the entire interval studied from 1 to 10% in parallel with water content which is varying between 20 and 60% (Fig. 3C). At the base of unit I, TOC and WC are relatively low and increase to high values in subunit IP. In unit II, they display a general decrease with three peaks during subunit IIa, IIb, and IIc. Both of them show minimum values with a general decreasing trend in unit III (Fig. 3C).

### 4.5. *P. lenticularis*

*P. lenticularis* is present from 15.35 to 14.34 m cd, i.e. between 13 and 11 ka cal. BP (Fig. 3E). In this latter interval, *P. lenticularis* is mostly abundant (Fig. 3E) in sediments, as we can observe on the Ca-mapping results in Fig. 5A.

## 5. Discussion

### 5.1. Micropumices

Micropumice is composed of highly microvesicular pyroclastic glass with very thin, translucent bubble walls of extrusive igneous rock. Image analysis and the assisted counting approach used here were helpful in making the count easier and more reliable. However, it is likely that such micropumices identification and counting still contain a bias that is difficult to assess for both techniques, especially in unit I because the facies matrix was saturated by glass and micropumices. Nevertheless, without thin-section image analysis in this interval, it is likely that the significance of the volcanic material in these sediments would have been missed.

This discovery raised the question of a potential modification of chemical composition of the sediment by micropumices. Their composition shows low content in Ti and Fe, as demonstrated by 275 analyses of glass shards from tephras in Laguna Potrok Aike (Wastegård et al., 2013), with TiO2 between 0.07 and 0.57 wt%, and FeOtot between 0.61 and 2.89 wt%, and point to a felsic source from the Andes. Moreover, the ratios between Ti and Fe and between Si and Ti are constant in micropumices. In our entire interval, the more the micropumices content is decreasing, the less Si and Ti are correlated: in unit I $R^2 = 0.73$, in unit II $R^2 = 0.42$, and in unit III $R^2 = 0.05$ (Fig. 9B). This points to a modulation effect by the micropumices. This is further supported by the increase of Ti and Fe from unit II to the end of unit III that is likely due the decrease in micropumices content (Fig. 3B and D). Moreover, when micropumices content increases during subunits IIa, IIb, and IIc, Ti and Fe are decreasing as well.

### 5.2. XRF proxies

#### 5.2.1. Calcium and manganese

To explain the variations in calcium and manganese in our sediment core, it is necessary to assess the different potential sources of these elements and processes affecting the deposition and preservation. Sources of calcium in lacustrine sediments at Laguna Potrok Aike, hence the primary source of $Ca^{2+}$ into the lake water, could result from the weathering of basaltic rocks in the catchment area (Haberzettl et al., 2005). Lacustrine calcareous

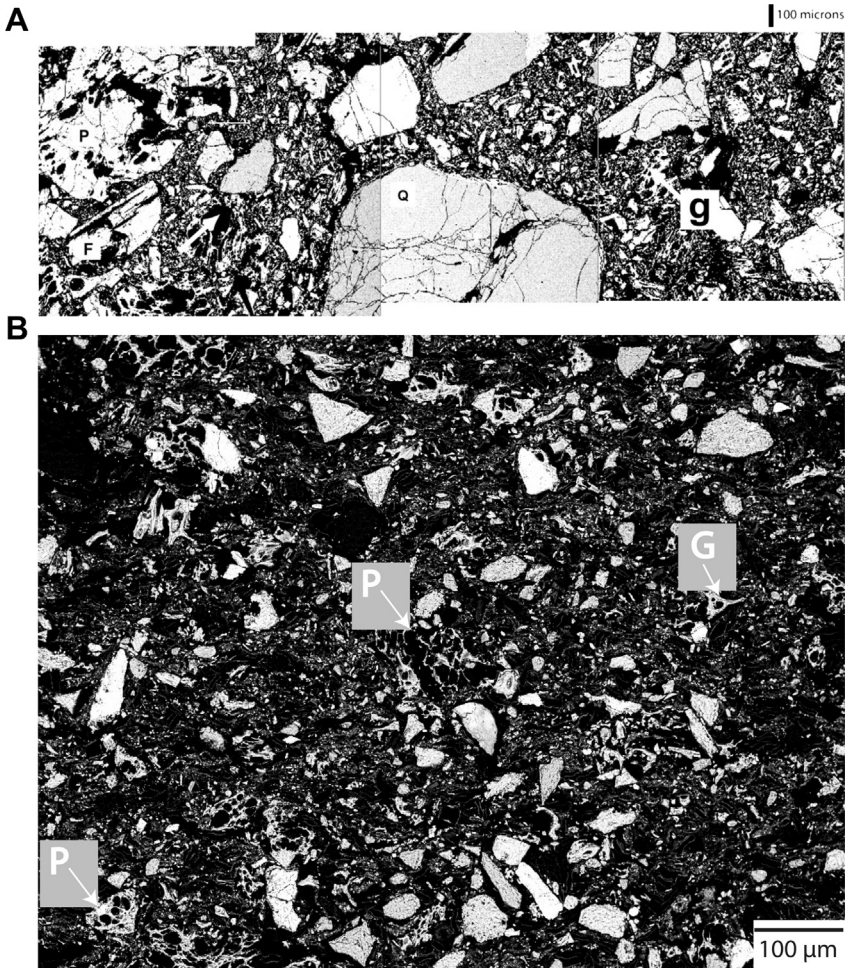


**Fig. 4.** Comparison of SEM images from Evans and Bradbury (2004) and a SEM–BSE-image for micropumices characterization. A: mosaic of backscattered scanning electron micrograph of nondeformed nonwelded tuff from the Horton Creek site. Large feldspar phenocrysts (F), vesiculated pumice lapilli (P), and quartz grains (Q) lie in a matrix of irregularly shaped glass shards and ash. Intragranular fractures in the quartz may be the result of rapid cooling from the caldera. Images acquired with 10 kV accelerating voltage (Evans and Bradbury, 2004); B: backscattered scanning electron image showing vesiculated micropumices (P) and irregular glass shards (G) at Potrok Aike.

sediments can be formed as a combination of five processes (Kelts and Hsü, 1978; Dean and Fouch, 1983): primary inorganic precipitation and sedimentation of carbonate minerals; inorganically precipitated carbonate (photosynthesis induced); biogenic carbonate; clastic input of allochthonous carbonates and/or post depositional changes or early diagenetic reactions producing carbonates.

In aquatic environment, manganese is mainly present as Mn(II) and Mn(IV). The transition from one form to another takes place by redox reactions which may be abiotic or of microbial origin. In case of a depletion of oxygen and nitrate, oxyhydroxides of manganese are reduced in freshwater sediment. Precipitates of reduced manganese can be found in the form of rhodochrosite (Friedl et al., 1997). Indeed, the chemistry of manganese is largely dependent on the pH value and redox potential, as $Mn^{2+}$ mainly precipitates as $MnCO_3$ (rhodochrosite) (Koinig et al., 2003). The main chemical factors that determine the cycle of sedimentary manganese are the oxygen content of the water column, the oxygen penetration into sediment and organic carbon flux to the benthic zone. Manganese is very soluble with respect to most inorganic ions, but in certain environments, such as interstitial waters (Robbins and Callender, 1975), it is possible to exceed the solubility product of rhodochrosite, $MnCO_3$.

Ca and Mn are well correlated during the Lateglacial interval described in this study with a coefficient of correlation $R^2 = 0.62$ (Fig. 9A). In unit II, three peaks of Ca and Mn co-occur in subunits a, b, and c (Fig. 3B). In this unit, Ca was interpreted as a *P. lenticularis* calcifications signal instead of autochthonous calcite precipitations (Haberzettl et al., 2007). Fig. 5A shows how calcium is mostly present in *P. lenticularis*. The latter is a green alga which lorica incorporates remarkable concentrations of $CaCO_3$ (Pocratsky, 1982; Steinberg and Klee, 1983; Giering et al., 1990), and occurs only at water temperature $> 15.8$ °C and preferentially in alkaline water, with a pH between 8.3 and 9.6 (Müller and Oti, 1981; Schlegel et al., 1998). In our records, maximum presence of *P. lenticularis* is between 15.34 and 14.44 m cd, i.e. 13 and 11.1 ka cal. BP (Fig. 3E). *P. lenticularis* is not present during Ca and Mn peak in unit IIa (Fig. 3B and E). It appears only at the end of the subunit IIa. To well understand the Ca and Mn signal during the subunit IIa, we have to consider all different $CaCO_3$ polymorphs detected until now. At Laguna Potrok Aike, these are: aragonitic shells of Limnaea sp., which are rare (Haberzettl et al., 2007), µm-sized calcite crystals, highly present during Holocene (Haberzettl et al., 2007), and ikaite (Oehlerich et al., 2013). The carbonate mineral ikaite, a calcium-carbonate hexahydrate ($CaCO_3 \cdot 6H_2O$), was found in the whole water column of the lake (Oehlerich et al., 2013) during austral winter 2008. The presence of ikaite is indicative of a low-temperature, anaerobic, organic-carbon-rich marine environment (Jansen et al., 1987). At Laguna Potrok Aike, different mechanisms were revealed (Oehlerich et al., 2013): during austral summer,

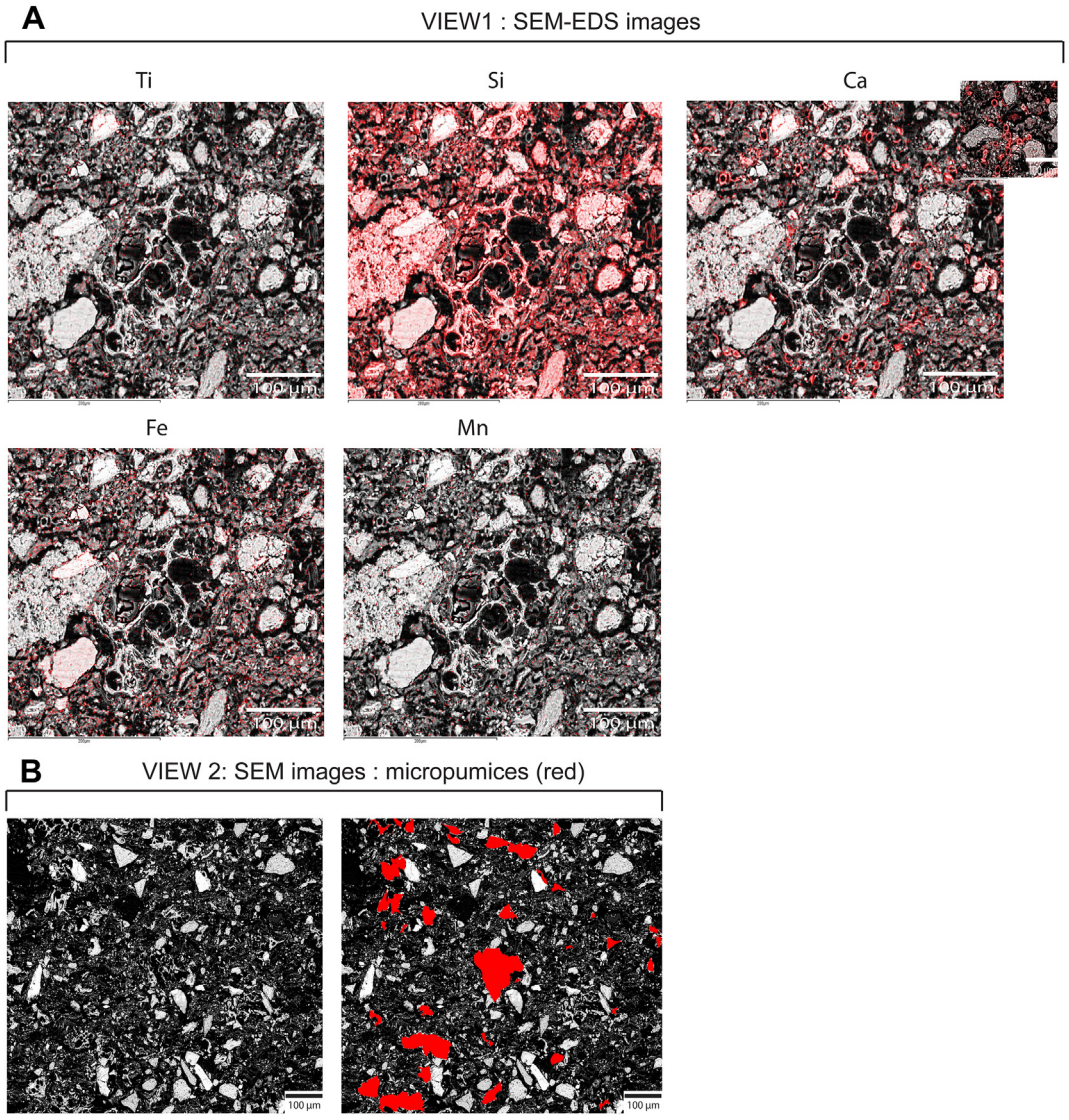


**Fig. 5.** A: SEM–EDS maps for 5 elements from view 1 in Fig. 3A. Red colour outlines the presence of each selected elements chosen on top of the BSE image. Red circles shapes "outline" *Phacotus lenticularis* on the Ca-map. B: SEM images (view 2 Fig. 3A) with micropumices coloured in red manually.

because of high evaporation rates and polymictic conditions, the entire water body enriches in dissolved $Ca^{2+}$ and $CO_3^{2-}$ (Oehlerich et al., 2013). Authigenic precipitation of more stable anhydrous $CaCO_3$ is inhibited by an elevated Mg and phosphate concentration (Oehlerich et al., 2013). Ikaite, a metastable mineral phase, is known to precipitate only at temperatures close to the freezing point and unstable at temperatures above 4 °C (Larsen, 1994; Rickaby et al., 2006). It is rapidly decomposes at temperatures above 4 °C and under certain conditions becomes pseudomorphed in calcite by *in situ* redistribution of the calcium and carbonate ions (Shearman et al., 1989).

The SEM investigation shows that Ca is partially present as detrital particles (Fig. 5A). Since $Mn^{2+}$ mainly precipitates as $MnCO_3$ (rhodochrosite) and, since the most common products of biomineralization are calcium and/or manganese compounds and the deposition of silica in intra- or extra-plasmatic organic matrices (Driessens and Verbeeck, 1990), it happens that Ca and Mn correlations could be linked to a $MnCO_3$ precipitation onto calcitic *P. lenticularis* lorica in a similar manner as reported by Boyle (1983) with foraminiferal shells in sediments where pore water $Mn^{2+}$ concentrations rise above the solubility product of the solid phase. Yet, the study of Nuttin et al. (2013), seems to undermine this interpretation because their mineralogical analysis using XRD did not reveal any rhodochrosite. However, we still consider this interpretation because the lack of rhodochrosite might be only due to the low sampling resolution of Nuttin's XRD study: only one XRD sample on twelve corresponds to depths where Mn peaks are observed in our study interval.

Total Organic Carbon cannot be used as proxy of organic carbon pulse or redox conditions in sediment in unit I because too many micropumices are present and are probably biasing any paleo-environmental reconstructions. However, in unit II, micropumices are less present (Fig. 3D) and the TOC could reflect organic carbon pulse or redox conditions. Currently, at Laguna Potrok Aike, wind speed enforces polymictic conditions and water column is not stratified (Zolitschka et al., 2006). Total Organic Carbon values are between 1 and 8% at depth corresponding to Mn peaks. The potential explanation for the preservation of Mn peaks associated to early diagenesis processes in well ventilated conditions with organic carbon pulse is not defendable here. Indeed, in these conditions,

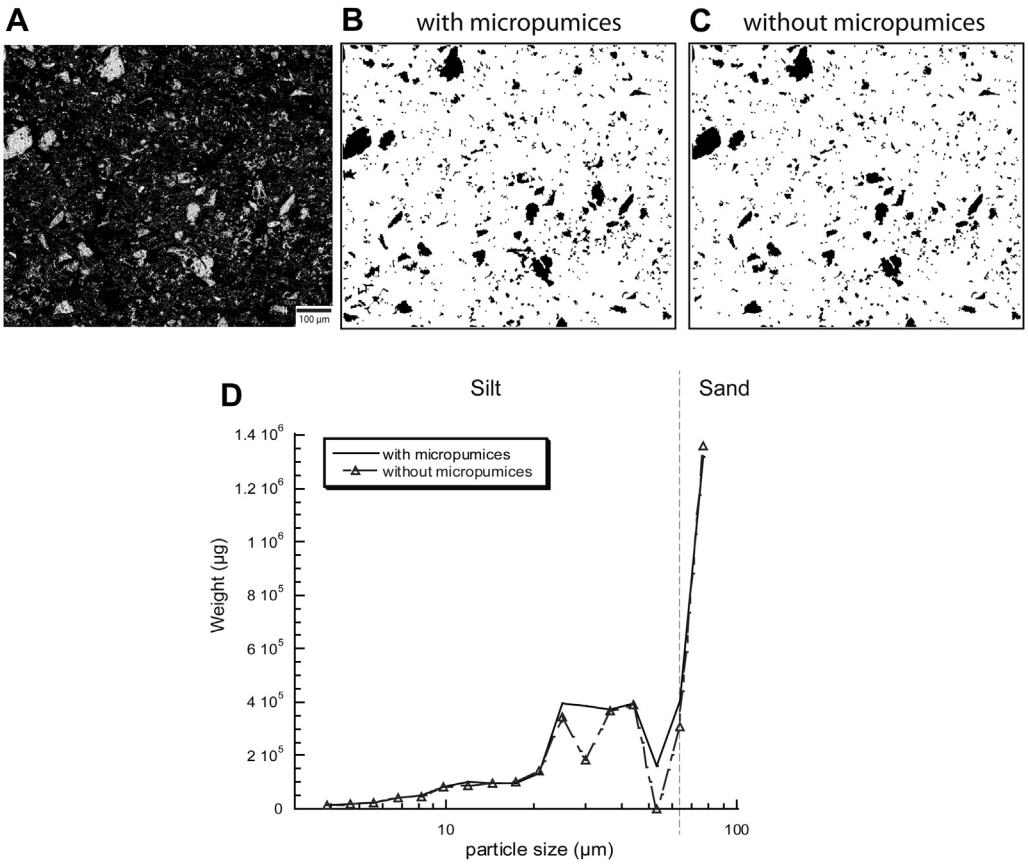


**Fig. 6.** A: SEM–BSE-image (1024*768 pixels, pixel size = 1 µm) from IA1 (see Fig. 3A) analysed conserving micropumices (B) and removing micropumices (C). Black pixels representing micropumices were removed from the black and white image using software tools. D: the logarithmic scale grain size plot of images with and without micropumices.

almost all organic carbon have to be consumed to preserve Mn peak (Gobeil et al., 2001) to such a degree that organic carbon should be between 0 and 0.5% only. Another explanation might be considered for the preservation of Mn peaks: if TOC peaks (Fig. 3C) correspond to micropumices peaks (Fig. 3D), may be a part of the original TOC signal was trapped within micropumices and was thus not available to be consumed by benthic activity. However, the interval with highest content in micropumices in unit I does not reveal Ca or Mn peak (Fig. 3B and D). Therefore, preservation of Mn peaks as diagenetic Mn-oxides associated to enrichment of dissolved $Mn^{2+}$ at the oxic-anoxic boundary in anoxic conditions at the water/sediment interface is more plausible. Thus, high TOC would reveal the non-degradation of organic matter in anoxic conditions. Only oxygen depletion in the deep basin, together with bacterial breakdown of detrital organic matter, can, at the sediment/water interface and deeper down, lead to conditions in favour of diagenetic Mn-oxides.

Summarizing this discussion, we infer that the first Ca/Si peak in subunit IIa (Fig. 3B) is either (1) derived from ikaite revealing colder conditions in the water column, either (2) represents primary inorganic precipitation indicating warmer conditions in the water column. The Ca/Si peaks during *P. lenticularis* occurrences, in subunits IIb and IIc, represent calcite precipitation on their lorica, in agreement with Haberzettl et al. (2007). Manganese would represent diagenetic Mn-oxides in a context of a low oxygenation in the deep basin in subunit IIa, IIb and IIc.

### 5.2.2. Titanium and iron

Titanium is generally used as an indicator of detrital input in lake sediment because it can reflect riverine clastic supply and by extension to determine paleohydrological variations. Demory et al. (2005) indeed demonstrated that Ti is released from Ti-bearing rocks by physical erosion (Cohen, 2003) and minerals containing Ti are not sensitive to chemical dissolution.

Concentrations in Ti and Fe oxides in rocks in the plateau-like basal lavas or volcanic rocks in the Pali Aike volcanic field (D'Orazio et al., 2000), and those of glass shards (Wastegård et al., 2013) are really dissimilar. Titanium and Fe concentrations in micropumices are 4–54 and 2–11 times lower respectively, than in any volcanic rocks from the Pali Aike Volcanic Field. Iron and Ti are correlated along Lateglacial times with an $R^2 = 0.94$ (Fig. 9A). This strong correlation between these two elements could be explained by two factors: first, detrital particles are rich in Ti and Fe and/or second, micropumices are poor in Ti and Fe. SEM–EDS mapping (Fig. 5A) clearly demonstrate how titanium and iron are supported by different phases. It seems that this correlation is mostly due to the constant concentrations of Ti and Fe in micropumices.

Our analysis therefore shows that Ti cannot be used as a paleohydrological indicator at Laguna Potrok Aike in the intervals where pumices or tephra are present.

It appears that the combined interpretation of Ca/Ti and Fe/Mn ratios in Haberzettl et al. (2007) needs to be re-evaluated in the light of the discovery of the micropumices and their chemical content. Concerning these ratios, another point might be considered. Indeed, based on the anti-correlation of these element ratios, Haberzettl et al. (2007) rationale was the following: if Ca/Ti represents autochthonous calcitic precipitation and/or *P. lenticularis* development, this ratio is related to lake level change (Haberzettl et al., 2007). The more the latter is high the more the lake level is low. Fe/Mn was interpreted as an indicator of paleoredox conditions, in so far as redox potential did not dropped below 100 mV. Haberzettl

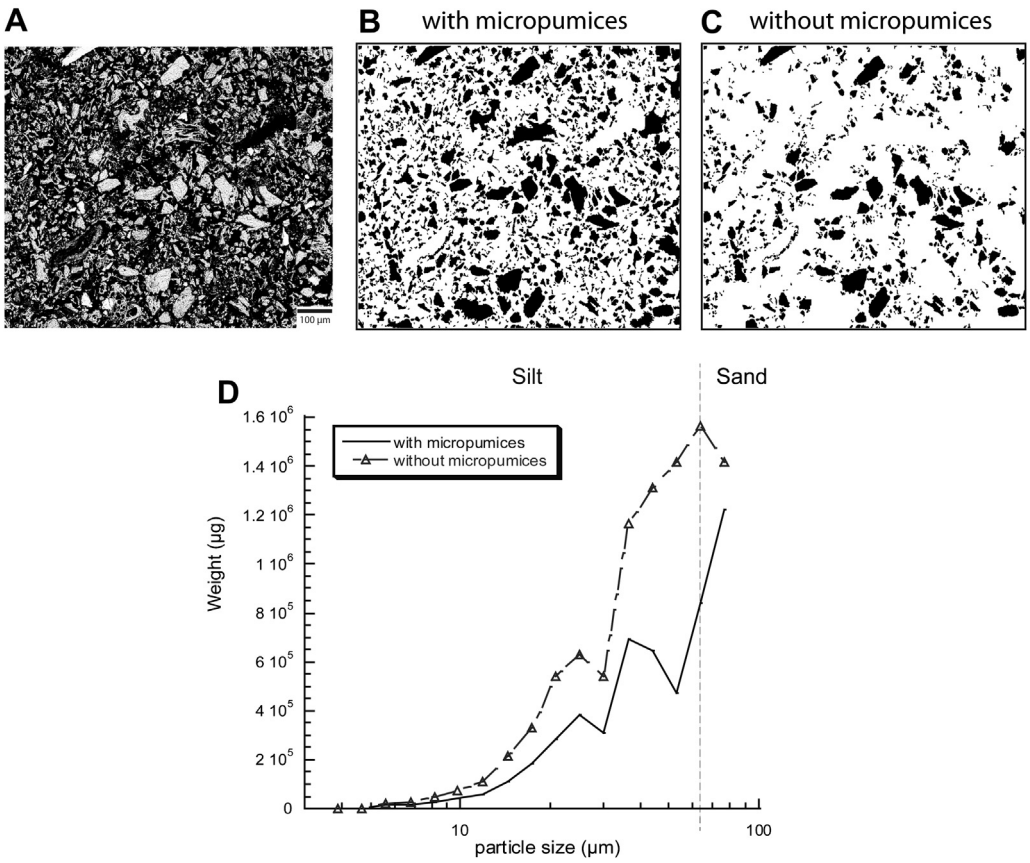


**Fig. 7.** A: SEM–BSE image (1024*768 pixels, pixel size = 1 µm) from IA2 (see Fig. 3A) analysed conserving micropumices (B) and removing micropumices (C). Black pixels representing micropumices were removed from the black and white image using software tools. D: the logarithmic scale grain size plot of images with and without micropumices.

et al. (2007) concluded that a lake level drop (Ca/Ti increase) creates water mixing bringing oxygen in water–sediment interface (Fe/Mn decrease). These two ratios are still very well anti-correlated with an $R^2 = 0.61$ over our interval of study.

However, the solubility of oxygen is greater in cold water than in warm water. According to the analyses of Zolitschka et al. (2006) between 2003 and 2005, water temperatures range from 4 to 14 °C during a year. If *P. lenticularis* occurrence reveals higher water temperature during 2000 years, oxygen supply in sediments could had been less important, as well as sediments oxygenation. Therefore, the Fe/Mn decrease interpreted as increased oxygenation of the water column due to a lake level drop concomitant to

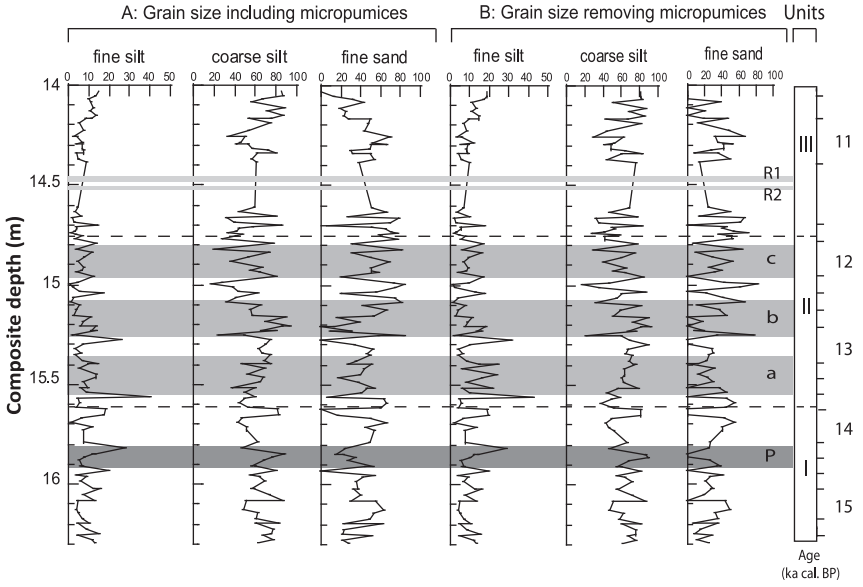


**Fig. 8.** Grain size including (A) or removing (B) micropumices.

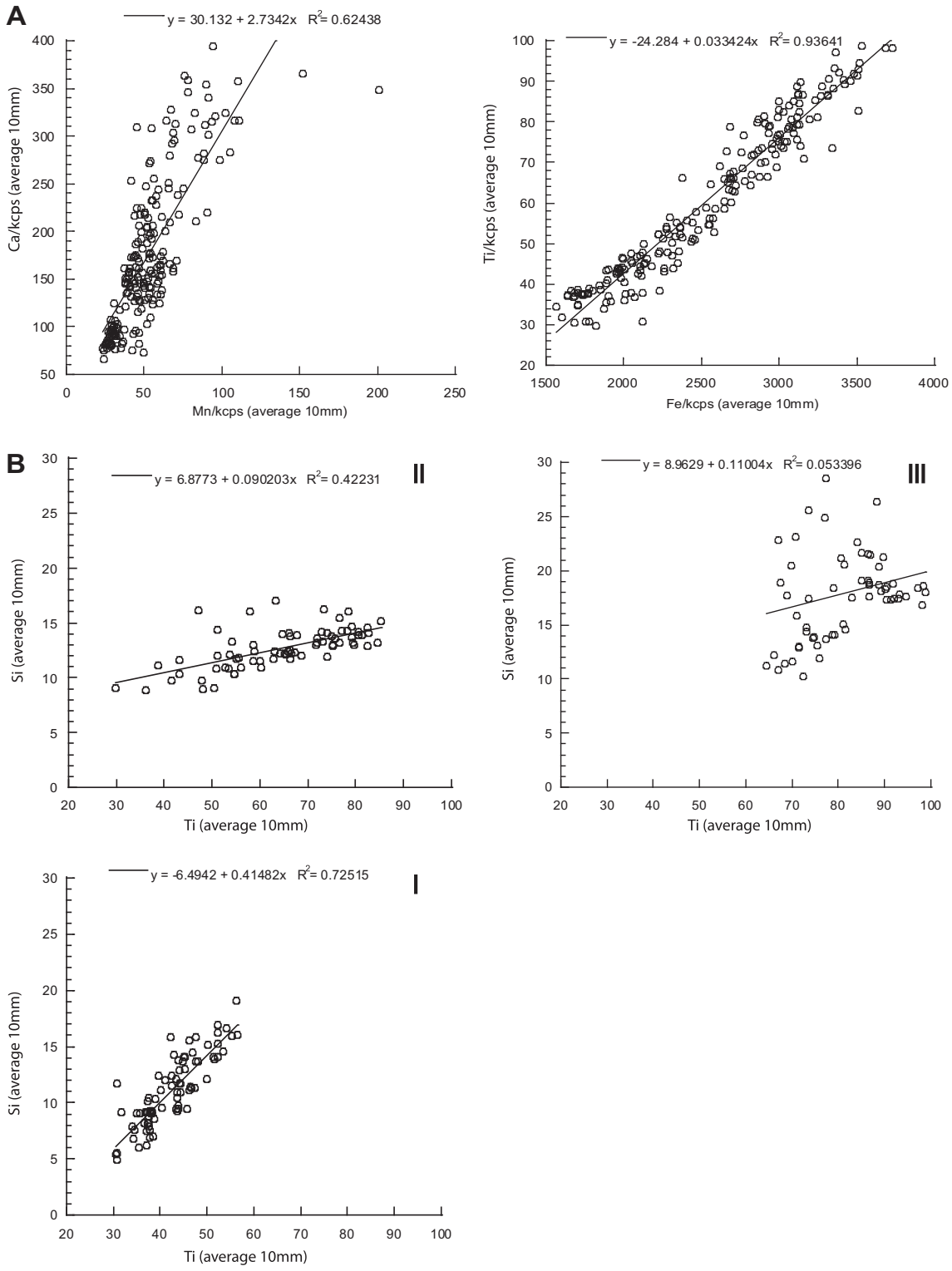


**Fig. 9.** A: scatter plots for Ca/kcps versus Mn/kcps and Ti/kcps versus Fe/kcps. B: scatter plots for Ti and Si for each unit (I, II, III) characterized in Fig. 3. Average 10 mm: points plotted represent mean values for each element every 10 mm.

a temperature increase (*P. lenticularis* occurrence) might have been less pronounced because of the decrease of oxygen solubility of the water column. These complex geochemical interactions give rise to a caution notice about the use of Fe/Mn ratio as an indicator of paleoredox conditions. Other points about Ca/Ti versus Fe/Mn signals should be considered. First, if Ca is related to Mn, because of *P. lenticularis,* and if Fe is related to Ti, because they are both important components of detrital input, then Ca/Ti and Fe/Mn are correlated. In consequence, correlations between Ca/Ti and Fe/Mn ratios are chemically driven and do not reveal any paleoenvironmental link. Second, we demonstrated previously that only oxygen depletion in the deep basin could explain manganese

behaviour from the ACR to the end of the YD. In anoxic conditions, redox potential should have certainly dropped below 100 mV, as it has been suggested as possible by Haberzettl et al. (2007). In consequence, Fe/Mn ratio cannot reveal changes in paleoredox conditions because in anoxic conditions within the sediment, both Fe and Mn should have been solubilized.

### 5.3. Influence of micropumices on μ-XRF, TOC and WC

Ti and Fe are very likely biased by micropumice between 15.2 and 11.8 ka cal. BP and cannot be used as a paleohydrological or a paleowind intensity proxy during Lateglacial. Ti is certainly not appropriate as a paleohydrological proxy or normalizer for Ca content. However, Si appears to be less influenced by the presence of micropumices. Fig. 5A shows that Ti is not abundant in sediments as well as in micropumices-rich intervals, contrary to Si, except in *P. lenticularis*-rich intervals. No correlation exists between Si and biogenic silica during the Lateglacial (Hahn et al., 2013), and mineralogical analysis attests 48–78% of quartz for Lateglacial times (Nuttin et al., 2013) indicating Si is not influenced by biogenic silica contents. For these reasons, Si is more suited as an indicator of the detrital input than Ti in this interval, and thus, Ca/Si should be used as an indicator of water lake temperature variations. However, as explained in Chapter 5.2.1, paleoenvironmental and palaeoclimatic context cannot be inferred only from its variations. Indeed, it could reveal (1) warmer temperature in the water column, because of *P. lenticularis* or primary inorganic precipitation, or (2) colder temperature in the water column, because of calcite derived from ikaite.

During the Lateglacial, TOC and WC are systematically correlated with inc/coh and micropumices content (Fig. 3B–D). Because of their vesicularity, micropumices can contain a large amount of organic carbon and water (Kitis et al., 2007). Therefore, it seems that interpretations derived from TOC, WC, and inc/coh need also to be considered cautiously in micropumices-rich intervals especially in unit I.

The grain-size of micropumices (Fig. 8) seems to be identical to the rest of the sediment within each analysed sample and don't seems to affect the general particle size trend as revealed by the strong correlation between grain size conserving or removing micropumices. Therefore, it appears that these micropumices behave like any other detrital particles composing the sediment, and are brought within the lake by similar sedimentary processes, being incorporated in the material available for sedimentation within the watershed. The 1.5 m of remobilized tephra and/or the Reclus eruption around 16 ka cal. BP have probably created an important deposit of micropumices around the lake, available for sedimentation by eolian or fluvial processes for at least 4000 years, according to our age model in Fig. 2 (Kliem et al., 2013).

### 5.4. Palaeoclimatological reconstruction

Sedimentological characterizations outlined that it is difficult to interpret μ-XRF results before 13.8 ka cal. BP, in the Lateglacial interval, because too many micropumices are present.

Generally, proxies can be interpreted as follows: Ca/Si, Mn and TOC peaks reveal a lake water body mostly stratified from 13.6 to 11.1 ka cal. BP, i.e. from the ACR to the end of the YD. Without strong westerlies, overturning of the water column would be limited to the epilimnion, producing an, at least periodic, anoxic hypolimnion allowing for the preservation of Mn-oxides and organic matter within the sediment. In this environment, during the YD, temperature in the epilimnion should be sufficiently warm for *P. lenticularis* to grow. In consequence, our evidences suggest colder conditions during the ACR, and a mild YD with cool summers without strong westerlies.

During the Holocene, the lowest lake level seemed to have occurred between 8.7 and 7.3 ka cal. BP mainly because of strong westerlies (Haberzettl et al., 2007; Mayr et al., 2007). This driest period of the Holocene was not favourable for the growth of *P. lenticularis*, as well as any other dry period of the Holocene as already pointed out by Haberzettl et al. (2007). Hence, these intense evaporation periods mainly driven by wind intensity, were also responsible for intense mixing the Laguna Potrok Aike water column, hence preventing its stratification and to reach temperatures warm enough to allow *P. lenticularis* to grow.

Therefore, the presence of *P. lenticularis* cannot be interpreted only in terms of maximum temperature. Indeed, at high latitudes in the Southern South Hemisphere, summer temperatures were substantially lower during the Lateglacial compared to the Holocene, and especially since 2 ka cal. BP, as indicated by summer insolation reconstruction at 52°S (Laskar et al., 2004; McGlone et al., 2010). However, *P. lenticularis* only appears during the Lateglacial. The strong correlation between Ca and Mn, the presence of *P. lenticularis* and high TOC values testify of outstanding environmental conditions since the last 16 ka cal. BP with lower wind speed.

More specifically, during the ACR, the non-*P. lenticularis* Ca peak, which one could be derived from ikaite (Oehlerich et al., 2013), reveals colder conditions than during the Younger Dryas. Diatoms and chironomids results in Massaferro et al. (2013) also uncover colder conditions during ACR than during the YD. This is also in agreement with Moreno et al. (2009) that delivered evidence for a glacier readvance and a cold episode during the ACR in southern Patagonia (50°S). McGlone et al. (2010) came to similar conclusion when suggesting that seasonality decreased in the latter part of the Lateglacial and early Holocene, with summers substantially cooler than present. The hypothesis of a mild climate with easterlies influence bringing more precipitation to Laguna Potrok Aike is preferentially considered. This is in agreement with atmospheric simulations developed by Pollock and Bush (2013). Their results attest of easterlies influences in the southern Patagonian steppe from the last glacial maximum until 9 ka cal. BP.

## 6. Conclusions

Our study revealed that the paleoenvironmental and palaeoclimatic interpretation of μ-XRF profiles gains much when supported by thin-section and SEM–EDS analyses to characterize the sediments.

At Laguna Potrok Aike, the interpretation of Fe and Ti as paleohydrological or paleowind indicators appears to be complicated during Lateglacial because of too many micropumices (up to 43% of particles between 4 and 100 μm) modify the geochemistry. The 1.5 m thick remobilized tephra and/or the Reclus tephra situated below our interval created an important source of micropumices around the lake that were eventually incorporated within the sediment by regular wind or fluvial processes variations. However, Si content was not affected by micropumices and by biogenic silica and can be used an indicator of the detritic input.

Paleoenvironmental and palaeoclimatological interpretations derived from Ca/Si ratio, Mn, TOC and *P. lenticularis* are consistent with those of other scientists involved in the SALSA and PASADO project and with the general pattern of climate evolution for southern South Hemisphere since the deglaciation developed by McGlone et al. (2010). We demonstrated that variations in the ventilation of the water column could explain preservation of manganese and Ca/Si peaks, *P. lenticularis* occurrence and high TOC values, from the ACR until the early Holocene, i.e. from 13.6 to

11.1 ka cal. BP. In Laguna Potrok Aike, the ACR chronozone were probably colder than the Younger Dryas chronozone.

## Acknowledgements

This research was supported by the International Continental Scientific Drilling Program (ICDP) in the framework of the "Potrok Aike Maar Lake Sediment Archive Drilling Project" (PASADO). Funding for drilling was provided by the ICDP, the German Science Foundation (DFG), the Swiss National Funds (SNF), the Natural Sciences and Engineering Research Council of Canada (NSERC), the the Swedish Research Council (VR) and the University of Bremen. NSERC Special Research Opportunities (SRO) provided further support for a PhD fellowship to GJ and analytical expenses. We thank Charles Gobeil for his intellectual input about geochemical interpretations, and the members of INRS-ETE for the valuable comments. We want to thank all reviewers for their necessary comments on the content and the form of our article. We also thank the staff of INTA Santa Cruz and Rio Dulce Catering as well as the Moreteau family and the DOSECC crew for their invaluable help in field logistics and drilling.

## Appendix A. Supplementary material

Supplementary material associated with this article can be found, in the online version, at http://dx.doi.org/10.1016/j.quascirev.2012.06.003.

## References

Basile, I., Grousset, F.E., Revel, M., Petit, J.R., Biscaye, P.E., Barkov, N.I., 1997. Patagonian origin of glacial dust deposited in East Antarctica (Vostok and Dome C) during glacial stages 2, 4 and 6. Earth and Planetary Science Letters 146 (3–4), 573–589.

Boyle, E.A., 1983. Manganese carbonate overgrowths on foraminifera tests. Geochimica et Cosmochimica Acta 47 (10), 1815–1819.

Cohen, A.S., 2003. Paleolimnology. The History and Evolution of Lake Systems. Oxford University Press, New York, 528 p.

Croudace, I.W., Rindby, A., Rothwell, R.G., 2006. ITRAX: Description and Evaluation of a New Multi-function X-ray Core Scanner. In: Geological Society, London, Special Publications, vol. 267(1), pp 51–63.

D'Orazio, M., Agostini, S., Mazzarini, F., Innocenti, F., Manetti, P., Haller, M.J., Lahsen, A., 2000. The Pali Aike volcanic field, Patagonia: slab-window magmatism near the tip of South America. Tectonophysics 321 (4), 407–427.

De Keyser, T.L., 1999. Digital scanning of thin sections and peels. Journal of Sedimentary Research 69 (4), 962–964.

Dean, W.E., Fouch, T.D., 1983. Lacustrine environments. In: Scholle, P.A., Debout, D., Moore, D. (Eds.), 1983. Carbonate Depositional Environments, vol. 33. The Am. Assoc. Pet. Geol. Mem., pp. 97–130.

Demory, F., Oberhänsli, H., Nowaczyk, N.R., Gottschalk, M., Wirth, R., Naumann, R., 2005. Detrital input and early diagenesis in sediments from Lake Baikal revealed by rock magnetism. Global and Planetary Change 46 (1–4), 145–166.

Driessens, F.C.M., Verbeeck, R.M.H., 1990. Biominerals. CRC Press, Boca Raton, Florida, p 417.

Endlicher, W., 1993. Klimatische Aspekte der Weidedegradation in Ost-Patagonien. Geographische Gesellschaft Trier, pp 91–103.

Eusterhues, K., Heinrichs, H., Schneider, J., 2005. Geochemical response on redox fluctuations in Holocene lake sediments, lake Steisslingen, Southern Germany. Chemical Geology 222 (1–2), 1–22.

Evans, J.P., Bradbury, K.K., 2004. Faulting and fracturing of nonwelded Bishop tuff, Eastern California: deformation mechanisms in very porous materials in the Vadose Zone. Vadose Zone Journal 3 (2), 602–623.

Fortin, D., Francus, P., Gebhardt, C., Hahn, A., Kliem, P., Ohlendorf, C., The PASADO Science Team, 2013. Density variability of the PASADO long composite record – method comparison and interpretation. Quaternary Science Reviews 71, 147–153.

Francus, P., 1998. An image-analysis technique to measure grain-size variation in thin sections of soft clastic sediments. Sedimentary Geology 121 (3–4), 289–298.

Francus, P., Karabanov, E., 2000. A computer-assisted thin-section study of Lake Baikal sediments: a tool for understanding sedimentary processes and deciphering their climatic signal. International Journal of Earth Sciences 89 (2), 260–267.

Francus, P., Asikainen, C.A., 2001. Sub-sampling unconsolidated sediments: a solution for the preparation of undisturbed thin-sections from clay-rich sediments. Journal of Paleolimnology 26 (3), 323–326.

Francus, P., Bradley, R.S., Abbott, M.B., Patridge, W., Keimig, F., 2002. Paleoclimate studies of minerogenic sediments using annually resolved textural patterns. Geophysical Research Letters 29 (20), 1998.

Francus, P., 2004. Image Analysis, Sediments and Paleoenvironments. Kluwer Academic Publishers, Dordrecht; Norwell, MA, p 330.

Francus, P., Nobert, P., 11-14th July 2007. An integrated computer system to acquire, process, measure and store images of laminated sediments. In: 4th International Limnogeology Congress, Barcelona, Spain.

Friedl, G., Wehrli, B., Manceau, A., 1997. Solid phases in the cycling of manganese in eutrophic lakes: new insights from EXAFS spectroscopy. Geochimica et Cosmochimica Acta 61 (2), 275–290.

Giering, B., Krienitz, L., Casper, S.J., Peschke, T., Raidt, H., 1990. LMund SEM-Beobachtungen an phacotus sphaericus (Wislouch) Giering nov. Star. (Chlamydophyceae, Phacotaceae). Archiv für Protistenkunde 138, 323–332.

Gilli, A., Anselmetti, F., Ariztegui, D., Bradbury, J., Kelts, K., Markgraf, V., McKenzie, J., 2001. Tracking abrupt climate change in the Southern Hemisphere: a seismic stratigraphic study of Lago Cardiel, Argentina (49°S). Terra Nova 13, 443–448.

Gilli, A., Anselmetti, F.S., Ariztegui, D., Beres, M., McKenzie, J.A., Markgraf, V., 2005a. Seismic stratigraphy, buried beach ridges and contourite drifts: the Late Quaternary history of the closed Lago Cardiel basin, Argentina (49°S). Sedimentology 52 (1), 1–23.

Gilli, A., Ariztegui, D., Anselmetti, F.S., McKenzie, J.A., Markgraf, V., Hajdas, I., McCulloch, R.D., 2005b. Mid-Holocene strengthening of the southern westerlies in South America – Sedimentological evidences from Lago Cardiel, Argentina (49°S). Global and Planetary Change 49 (1–2), 75–93.

Glasser, N.F., Harrison, S., Winchester, V., Aniya, M., 2004. Late Pleistocene and Holocene palaeoclimate and glacier fluctuations in Patagonia. Global and Planetary Change 43 (1–2), 79–101.

Gobeil, C., Sundby, B., Macdonald, R.W., Smith, J.N., 2001. Recent change in organic carbon flux to Arctic Ocean deep basins: evidence from acid volatile sulfide, manganese and rhenium discord in sediments. Geophysical Research Letters 28 (9), 1743–1746.

Guilderson, T.P., Burckle, L., Hemming, S., Peltier, W.R., 2000. Late Pleistocene sea level variations derived from the Argentine Shelf. Geochemistry Geophysics Geosystems 1. Paper number 2000GC000098.

Guyard, H., Chapron, E., St-Onge, G., Anselmetti, F.S., Arnaud, F., Magand, O., Francus, P., Mélières, M.A., 2007. High-altitude varve records of abrupt environmental changes and mining activity over the last 4000 years in the Western French Alps (Lake Bramant, Grandes Rousses Massif). Quaternary Science Reviews 26, 2644–2660.

Haberzettl, T., Fey, M., Lücke, A., Maidana, N., Mayr, C., Ohlendorf, C., Schäbitz, F., Schleser, G.H., Wille, M., Zolitschka, B., 2005. Climatically induced lake level changes during the last two millennia as reflected in sediments of Laguna Potrok Aike, southern Patagonia (Santa Cruz, Argentina). Journal of Paleolimnology 33 (3), 283–302.

Haberzettl, T., Corbella, H., Fey, M., Janssen, S., Lücke, A., Mayr, C., Ohlendorf, C., Schäbitz, F., Schleser, G.H., Wille, M., Wulf, S., Zolitschka, B., 2007. Lateglacial and Holocene wet-dry cycles in southern Patagonia: chronology, sedimentology and geochemistry of a lacustrine record from Laguna Potrok Aike, Argentina. The Holocene 17 (3), 297–310.

Haberzettl, T., Anselmetti, F., Bowen, S., Fey, M., Mayr, C., Zolitschka, B., Ariztegui, D., Mauz, B., Ohlendorf, C., Kastner, S., Lücke, A., Schäbitz, F., Wille, M., 2009. Late Pleistocene dust deposition in the Patagonian steppe – extending and refining the paleoenvironmental and tephrochronological record from Laguna Potrok Aike back to 55 ka. Quaternary Science Reviews 28, 2927–2938.

Hahn, A., Kliem, P., Ohlendorf, C., Zolitschka, B., Rosén, P., The PASADO Science Team, 2013. Climate induced changes in the carbonate and organic content of Laguna Potrok Aike sediments during the past 50 ka inferred from infrared spectroscopy. Quaternary Science Reviews 71, 154–166.

Haug, G.H., Günther, D., Peterson, L.C., Sigman, D.M., Hughen, K.A., Aeschlimann, B., 2003. Climate and the collapse of Maya civilization. Science 299 (5613), 1731–1735.

Jansen, J.H.F., Woensdregt, C.F., Kooistra, M.J., van der Gaast, S.J., 1987. Ikaite pseudomorphs in the Zaire deep-sea fan: an intermediate between calcite and porous calcite. Geology 15 (3), 245–248.

Jenkins, R., 1999. X-ray Fluorescence Spectrometry, Chemical Analysis: a Series of Monographs on Analytical Chemistry and Its Applications, vol. 152, 12 p.

Jouzel, J., Lorius, C., Petit, J.R., Genthon, C., Barkov, N.I., Kotlyakov, V.M., Petrov, V.M., 1987. Vostok ice core: a continuous isotope temperature record over the last climatic cycle (160,000 years). Nature 329, 403–408.

Kelts, K., Hsü, K.J., 1978. Freshwater Carbonate Sedimentation. Chemistry, Geology, Physics. Springer-Verlag, New York, pp 295–323.

Kitis, M., Kaplan, S.S., Karakaya, E., Yigit, N.O., Civelekoglu, G., 2007. Adsorption of natural organic matter from waters by iron coated pumice. Chemosphere 66 (1), 130–138.

Kliem, P., Enters, D., Hahn, A., Ohlendorf, C., Lisé-Pronovost, A., St-Onge, G., Wastegård, S., Zolitschka, B., The PASADO Science Team, 2013. Lithology, radiocarbon dating and sedimentological interpretation of the 51 ka BP lacustrine record from Laguna Potrok Aike, southern Patagonia. Quaternary Science Reviews 71, 54–69.

Koinig, K.A., Shotyk, W., Lotter, A.F., Ohlendorf, C., Sturm, M., 2003. 9000 years of geochemical evolution of lithogenic major and trace elements in the sediment of an alpine lake – the role of climate, vegetation, and land-use history. Journal of Paleolimnology 30 (3), 307–320.

Krumbein, W.C., Sloss, L.L., 1963. Stratigraphy and Sedimentation, second ed. Freeman, San Francisco.

Labeyrie, L., Jouzel, J., Lévi, C., Cortijo, E., 2004. Changements abrupts dans un monde glaciaire. Comptes Rendus Geosciences 336 (7–8), 721–732.
Lamoureux, S.F., 1994. Embedding unfrozen lake sediments for thin section preparation. Journal of Paleolimnology 10 (2), 141–146.
Lamoureux, S.F., Bollmann, J., 2004. Image acquisition. In: Francus, P. (Ed.), Image Analysis, Sediments and Paleoenvironments. Springer Science+Business Media, Dordrecht, pp. 11–34.
Larsen, D., 1994. Origin and palaeoenvironmental significance of calcite pseudomorphs after ikaite in the Oligocene Creede Formation, Colorado. Journal of Sedimentological Research 64, 593–603.
Laskar, J., Robutel, P., Joutel, F., Gastineau, M., Correia, A.C.M., Levrard, B., 2004. A long-term numerical solution for the insolation quantities of the Earth. Astronomy and Astrophysics 428, 261–285.
Lisé-Pronovost, A., St-Onge, G., Gogorza, C., Zolitschka, B., The PASADO Science Team, 2013. High-resolution paleomagnetic secular variation and relative paleointensity since the Late Pleistocene in Southern South America. Quaternary Science Reviews 71, 91–108.
Lowe, J.J., Rasmussen, S.O., Björck, S., Hoek, W.Z., Steffensen, J.P., Walker, M.J.C., Yu, Z.C., 2008. Synchronisation of palaeoenvironmental events in the North Atlantic region during the last termination: a revised protocol recommended by the INTIMATE group. Quaternary Science Reviews 27 (1–2), 6–17.
Markgraf, V., Bradbury, J.P., Schwalb, A., Burns, S.J., Stern, C., Ariztegui, D., Gilli, A., Anselmetti, F.S., Stine, S., Maidana, N., 2003. Holocene palaeoclimates of southern Patagonia: limnological and environmental history of Lago Cardiel, Argentina. The Holocene 13 (4), 581–591.
Massaferro, J., Recasens, C., Larocque-Tobler, I., Maidana, N.I., 2013. Major lake level fluctuations and climate changes for the past 16,000 years as reflected by diatoms and chironomids preserved in the sediment of Laguna Potrok Aike, southern Patagonia. Quaternary Science Reviews 71, 167–174.
Mayr, C., Fey, M., Haberzettl, T., Janssen, S., Lücke, A., Maidana, N.I., Ohlendorf, C., Schäbitz, F., Schleser, G.H., Struck, U., Wille, M., Zolitschka, B., 2005. Palaeoenvironmental changes in southern Patagonia during the last millennium recorded in lake sediments from Laguna Azul (Argentina). Palaeogeography, Palaeoclimatology, Palaeoecology 228 (3–4), 203–227.
Mayr, C., Lücke, A., Stichler, W., Trimborn, P., Ercolano, B., Oliva, G., Ohlendorf, C., Soto, J., Fey, M., Haberzettl, T., Janssen, S., Schäbitz, F., Schleser, G.H., Wille, M., Zolitschka, B., 2007. Precipitation origin and evaporation of lakes in semi-arid Patagonia (Argentina) inferred from stable isotopes ($\delta^{18}O$, $\delta^{2}H$). Journal of Hydrology 334 (1–2), 53–63.
Moreno, P.I., Kaplan, M.R., Francois, J.P., Villa-Martinez, R., Moy, C.M., Stern, C.R., Kubik, P.W., 2009. Renewed glacial activity during the Antarctic cold reversal and persistence of cold conditions until 11.5 ka in southwestern Patagonia. Geology 37 (4), 375–378.
McGlone, M.S., Turney, C.S.M., Wilmshurst, J.M., Renwick, J., Pahnke, K., 2010. Divergent trends in land and ocean temperature in the Southern Ocean over the past 18,000 years. Nature Geoscience 3 (9), 622–626.
Müller, G., Oti, M., 1981. The occurrence of calcified planktonic green algae in freshwater carbonates. Sedimentology 28 (6), 897–902.
Nuttin, L., Preda, M., Francus, P., Hillaire-Marcel, C., The PASADO Science Team, 2013. Clay and early diagenetic (vivianite) minerals in the Laguna Potrok Aike sediment sequence. Quaternary Science Reviews 71, 109–118.
Oehlerich, M., Mayr, C., Griesshaber, E., Kastner, S., Lücke, A., Oeckler, O.M., Ohlendorf, C., Schmahl, W.W., Zolitschka, B, 2013. Ikaite precipitation in a lacustrine environment – implications for paleoclimatic studies using carbonates from Laguna Potrok Aike (Patagonia, Argentina). Quaternary Science Reviews 71, 46–53.
Ohlendorf, C., Gebhardt, C., Hahn, A., Kliem, P., Zolitschka, B., 2011. The PASADO core processing strategy – a proposed new protocol for sediment core treatment in multidisciplinary lake drilling projects. Sedimentary Geology 239 (1–2), 104–115.
Pedro, J.B., van Ommen, T.D., Rasmussen, S.O., Morgan, V.I., Chappellaz, J., Moy, A.D., Masson-Delmotte, V., Delmotte, M., 2011. The last deglaciation: timing the bipolar seesaw. Climate of the Past Discussions 7, 671–683.
Pocratsky, L.A., 1982. Nutritional, chemical and ultrastructural characterization of the lorica and extracellular mucilage of *Phacotus lenticularis* (Phacotaceae, Volvocales). PhD dissertation, University of Tennessee, Knoxville.
Pollock, T., Bush, A., 2013. Atmospheric simulations of the present and past climate of southern South America. Quaternary Science Reviews 71, 219–228.
Revel-Rolland, M., De Deckker, P., Delmonte, B., Hesse, P.P., Magee, J.W., Basile-Doelsch, I., Grousset, F., Bosch, D., 2006. Eastern Australia: a possible source of dust in East Antarctica interglacial ice. Earth and Planetary Science Letters 249 (1–2), 1–13.
Rickaby, R.E.M., Shaw, S., Bennitt, G., Kennedy, H., Zabel, M., Lennie, A., 2006. Potential of ikaite to record the evolution of oceanic $\delta^{18}O$. Geology 34, 497–500.
Robbins, J.A., Callender, E., 1975. Diagenesis of manganese in lake Michigan sediments. American Journal of Science 275 (5), 512–533.
Röthlisberger, R., Mulvaney, R., Wolff, E.W., Hutterli, M.A., Bigler, M., Sommer, S., Jouzel, J., 2002. Dust and sea salt variability in central East Antarctica (Dome C) over the last 45 kyrs and its implications for southern high-latitude climate. Geophysical Research Letters 29 (20), 1963.
Schlegel, I., Koschel, R., Krienitz, L., 1998. On the occurrence of *Phacotus lenticularis* (Chlorophyta) in lakes of different trophic state. Hydrobiologia 369-370 (0), 353–361.
Schneider, C., Glaser, M., Kilian, R., Santana, A., Butorovic, N., Casassa, G., 2003. Weather observations across the southern Andes at 53°S. Physical Geography 24, 97–119.
Shearman, D.J., McGugan, A., Stein, C., Smith, A.J., 1989. Ikaite, $CaCO_3s6H_2O$, precursor of the thinolites in the Quaternary tufas and tufa mounds of the Lahontan and Mono lake basins, western United States. Geological Society of America Bulletin 101 (7), 913–917.
Siani, G., Colin, C., Michel, E., Carel, M., Richter, T., Kissel, C., Dewilde, F., 2010. Late glacial to Holocene terrigenous sediment record in the northern Patagonian margin: paleoclimate implications. Palaeogeography, Palaeoclimatology, Palaeoecology 297 (1), 26–36.
Skewes, M.A., 1978. Geologia, petrologia, quimismo y origen de los volcanes del area de Pali-Aike, Magallanes, Chile. Anales del Instituto de la Patagonia 9, 95–106.
Steinberg, C., Klee, R., 1983. Röntgenmikroanalyse der Schale einer einzelligen Grfinalge: Chemismus einer Phacotus lendneri-Schale. Mikrokosmos 72, 170–173.
Sugden, D.E., McCulloch, R.D., Bory, A.J.M., Hein, A.S., 2009. Influence of Patagonian glaciers on Antarctic dust deposition during the last glacial period. Nature Geoscience 2 (4), 281–285.
Unkel, I., Björck, S., Wohlfarth, B., 2008. Deglacial environmental changes on Isla de los Estados (54.4°S), southeastern Tierra del Fuego. Quaternary Science Reviews 27 (15–16), 1541–1554.
Villa-Martínez, R., Moreno, P.I., 2007. Pollen evidence for variations in the southern margin of the westerly winds in SW Patagonia over the last 12,600 years. Quaternary Research 68 (3), 400–409.
Wastegård, S., Veres, D., Kliem, P., Ohlendorf, C., Zolitschka, B., and the PASADO science team, 2013. Towards a late Quaternary tephrochronological framework for the southernmost part of South America - the Laguna Potrok Aike tephra record. Quaternary Science Reviews 71, 81–90.
Wentworth, C.K., 1922. A scale of grade and class terms for clastic sediments. Journal of Geology 30, 377–392.
Whitlock, C., Moreno, P.I., Bartlein, P., 2007. Climatic controls of Holocene fire patterns in southern South America. Quaternary Research 68 (1), 28–36.
Wille, M., Maidana, N.I., Schäbitz, F., Fey, M., Haberzettl, T., Janssen, S., Lücke, A., Mayr, C., Ohlendorf, C., Schleser, G.H., Zolitschka, B., 2007. Vegetation and climate dynamics in southern South America: the microfossil record of Laguna Potrok Aike, Santa Cruz, Argentina. Review of Palaeobotany and Palynology 146 (1–4), 234–246.
Zolitschka, B., Schäbitz, F., Lücke, A., Corbella, H., Ercolano, B., Fey, M., Haberzettl, T., Janssen, S., Maidana, N., Mayr, C., Ohlendorf, C., Oliva, G., Paez, M.M., Schleser, G.H., Soto, J., Tiberi, P., Wille, M., 2006. Crater lakes of the Pali Aike volcanic field as key sites for paleoclimatic and paleoecological reconstructions in southern Patagonia, Argentina. Journal of South American Earth Sciences 21 (3), 294–309.
Zolitschka, B., Anselmetti, F., Ariztegui, D., Corbella, H., Francus, P., Ohlendorf, C., Schäbitz, F., Team, T. P. S. D., 2009a. The Laguna Potrok Aike scientific drilling project PASADO (ICDP expedition 5022). Scientific Drilling 8.
Zolitschka, B., Anselmetti, F.S., Ariztegui, D., Corbella, H., Francus, P., Gebhardt, A.C., Hahn, A., Kliem, P., Lücke, A., Ohlendorf, C., Schäbitz, F., 2009b. Deep drilling at Laguna Potrok Aike, Argentina: recovery of a paleoclimate record for the last glacial from the southern hemisphere. Eos Transactions, American Geophysical Union 90 (52), Fall Meet. Suppl., Abstract PP14A-10.